

# Synthesis of 1-D ZnO nanorods and polypyrrole/1-D ZnO nanocomposites for photocatalysis and gas sensor applications

PRITAM PATIL<sup>1</sup>, GANESH GAIKWAD<sup>1</sup>, D R PATIL<sup>2</sup> and JITENDRA NAIK<sup>1,\*</sup>

<sup>1</sup>Department of Chemical Engineering, University Institute of Chemical Technology, North Maharashtra University, Jalgaon 425001, India

<sup>2</sup>Bulk and Nanomaterials Research Laboratory, Rani Laxmibai Mahavidyalaya Parola, Jalgaon 425111, India

MS received 5 June 2015; accepted 28 December 2015

**Abstract.** 1-D ZnO nanorods and PPy/1-D ZnO nanocomposites were prepared by the surfactant-assisted precipitation and *in situ* polymerization method, respectively. The synthesized nanorods and nanocomposites were characterized by UV–Vis spectrophotometer, Fourier transform-infrared spectroscopy (FTIR), X-ray diffraction (XRD) and field emission scanning electron microscope (FE-SEM), which gave the evidence of 1-D ZnO nanorods, polymerization of pyrrole monomer and strong interaction between PPy and 1-D ZnO nanorods, respectively. Photocatalytic activity of 1-D ZnO nanorods was conducted by 3<sup>3</sup> level full-factorial design to evaluate the effect of three independent process variables viz., dye concentration (crystal violet), catalyst concentration (1-D ZnO nanorods) and the reaction time on the preferred response: photodegradation efficiency (%). The PPy/1-D ZnO nanocomposites were used for the sensing of NH<sub>3</sub>, LPG, CO<sub>2</sub> and H<sub>2</sub>S gases, respectively, at room temperature. It was observed that PPy/1-D ZnO nanocomposites with different 1-D ZnO nanorod weight ratios (15 and 25%) had better selectivity and sensitivity towards NH<sub>3</sub> at room temperature.

**Keywords.** 1-D ZnO nanorods; PPy/1-D ZnO nanocomposites; photocatalytic activity; sensitivity.

## 1. Introduction

The synthesis of zinc oxide (ZnO) nanostructures such as nanoparticles, nanowires, nanorods, etc., has gained increasing research importance due to their unique properties and potential applications in various fields, such as gas sensing, solar cell, microelectronics, pharmaceuticals, photovoltaic and catalysis [1–9]. In the past two decades, ZnO nanostructures have prominent attribute because of its stability, wide band gap energy of 3.37 eV and large excitation binding energy of 60 meV at room temperature [10–13]. In addition, ZnO nanostructures offer a larger surface area to volume ratio than nanoparticulate thin films, owing to this characteristic advantage, it plays an important role in photodegradation [14]. However, this property has made ZnO as one of the most appealing photocatalyst semiconductor material for the degradation of organic pollutants in water under UV source. As a family of catalyst materials, ZnO nanostructures have been successfully prepared by variety of synthetic techniques. Among these techniques, the well-known precipitation method [15] is more useful and cost effective method. Kumar *et al* [16] prepared ZnO nanorods by a precipitation method with zinc sulphate and sodium hydroxide as starting materials followed by calcination. In this study, we use precipitation method for the synthesis of 1-D ZnO nanorod. The shape and size controlled 1-D ZnO nanorod synthesis is quite

difficult via a precipitation method, because the growth rate is too fast for the precursor to control the size. To overcome this difficulty, CTAB used as a structure directing surfactant [17].

The output of textile or dyestuff industries consists of coloured wastewater and dyes have more impact on the environment [18]. Among the wide range of dyes, crystal violet is a triphenylmethane dye which is highly toxic and carcinogenic [18,19]. Many techniques involving reverse osmosis, flocculation, chemical oxidation and reduction, electrochemical treatment and photocatalysis have been investigated for the treatment of crystal violet (CV) wastewater [20]. Of these, semiconductor-assisted photocatalysis has a prominent attribute because it is very effective to treat pollutants in both gas and liquid phases [21].

In this era with increased presence of pollutant gases in the atmosphere, it has become very essential to detect hazardous gases in standpoint of human safety measures. ZnO is a strong candidate for monitoring lethal gases because of its high electrochemical stability, good resistivity and excellent sensitivity towards gas pollutants [22]. Still, high operating temperature (350–450°C) of ZnO limits its real-time application. Conducting polymers (CPs) also show attractive gas sensing properties. Polypyrrole (PPy) is environmentally stable, can be easily prepared by chemical or electrochemical oxidative polymerization and have higher conductivity than other CPs [23]. However, metal oxide conducting polymer composites have been found to indicate smart sensing properties. PPy is a p-type material, while ZnO is n-type of material by tailoring this inorganic–organic composite, it is possible

\* Author for correspondence (jitunaik@gmail.com)

to make tunable conductivity sensors for better selectivity [24]. Some well-known materials for NH<sub>3</sub> gas sensing are ZnO, modified-ZnO [25], polyaniline [26], polypyrrole [27], Au and MoO<sub>3</sub>-modified WO<sub>3</sub> [28,29], Pt and SiO<sub>2</sub>-doped SnO<sub>2</sub> [30], etc. Various ammonia sensors reported, basically work at higher temperature such as 350°C, but it is inconvenient to attain such high temperature while sensing. So, the sensors operable at room temperature are needed. The electrolytic techniques using diaphragm electrodes are generally used for the detection of ammonia. However, this method is expensive and does not have sufficient response and selectivity for ammonia [31]. Another technique utilizes Pd-metal oxide semiconductor MOS device. This device is sensitive to ammonia, but it suffers from selectivity. So, semiconducting oxide sensors are considered here. Few sensor models are also available for detecting ammonia gas. They are: Figaro gas sensor model-TGS 824 (detection range 300 ppm) and Sierra gas monitor model-CM 99-447 (electrochemical type, detection range 200 ppm).

Despite of high sensitivity, selectivity and long-term stability, the main drawback of such sensors is that they operate at high working temperature (>300°C). Also, the use of metal additives likes Pt, Pd, Au, Ag, etc. in base material like ZnO for the modification, increases the cost of the sensors. Therefore, the applicability of these sensors remains limited. Hence, the sensors operable at room temperature with the low-cost metal additives must be developed for large applicability. In the present work, we have used 1-D ZnO nanorod for photocatalytic degradation of crystal violet and its nanocomposite with polypyrrole to develop the room temperature ammonia sensors.

## 2. Materials and methods

### 2.1 Materials

Zinc sulphate heptahydrate (ZnSO<sub>4</sub>·7H<sub>2</sub>O, Merck), Iron chloride (FeCl<sub>3</sub>, Merck) and sodium hydroxide (NaOH, S.D. Fine Chem. Ltd) were used as received. Cetyltrimethylammonium bromide (CTAB, Spectrochem) was used as the stabilizing agent, pyrrole monomer (Sigma-Aldrich) was used for the synthesis of PPy/ZnO nanocomposite. All other chemicals were of analytical grade and used as received. Double-distilled water was used throughout the experiments.

### 2.2 Synthesis of 1-D ZnO nanorods

1-D ZnO nanorods were synthesized by the surfactant-assisted precipitation method followed by calcination. In brief, ZnSO<sub>4</sub>·7H<sub>2</sub>O and NaOH were taken as the precursors of the synthesis process. Both precursors were dissolved separately in double-distilled water to obtain molar ratio (1 : 1 to 1 : 4) of solutions. ZnSO<sub>4</sub>·7H<sub>2</sub>O solution (50 ml) was added drop by drop and vigorously stirred in NaOH and CTAB solution. The addition rate of ZnSO<sub>4</sub>·7H<sub>2</sub>O solution was maintained using a syringe pump (Infusor, Universal Medical

Instruments, India). The white precipitate product obtained, filtered, washed and dried at 70°C in an oven for 2 h. Finally, the resultant product was calcined at 200°C for 4 h [32,33].

### 2.3 Synthesis of PPy/1-D ZnO nanocomposite

PPy/1-D ZnO nanocomposite was synthesized by *in situ* polymerization [34] of pyrrole monomer in the presence of 1-D ZnO nanorods. 1-D ZnO was dispersed in 50 ml of 0.35 M FeCl<sub>3</sub> solution for 10 min using bath sonicator. Then, 1 ml of pyrrole monomer added drop by drop into the solution under stirring. Vigorous stirring of the mixture for 3 h resulted in a black coloured solution, which was filtered and washed repeatedly with double-distilled water. The solid product obtained was dried in an air oven for 4 h.

### 2.4 Characterization

Degradation performance of CV dye was examined by UV-Vis spectrophotometer (HITACHI U-2900, Tokyo, Japan). The surface morphology of the products was examined by scanning electron microscopy (FESEM-S 4800, Hitachi, Japan) at a working distance of 8.6–8.8 mm and accelerating voltage of 15.0 kV. The components of materials were measured by a FTIR spectrophotometer (FTIR-8400; Shimadzu, Asia Pacific Pvt. Ltd, Singapore) by potassium bromide pellet method. For that, sample (1 mg) was mixed with KBr (40 mg) and compressed into a disc in a manual press. Spectra were recorded in the wavelength region of 4000–400 cm<sup>-1</sup>. The physical nature of the samples was examined by an X-ray diffractometer (Bruker, D8 Advanced, Germany) with CuKα radiation ( $\lambda = 1.5406 \text{ \AA}$ ). The anode X-ray tube was operated at 40 kV and 40 mA. The samples were analysed over the angle range 0–80° on the 2θ scale at a step size of 0.03 s<sup>-1</sup>.

### 2.5 Photodegradation experiments

The photodegradation of CV dye was performed under UV light source. The aqueous suspension of CV was prepared by adding a known quantity of ZnO nanorod powder into a solution containing a suitable concentration of CV. Then, the suspension was magnetically stirred in the dark for 1 h to allow an adsorption–desorption equilibrium between CV and the surface of the 1-D ZnO nanorod catalyst. Irradiation was carried out in a quartz cell located at 10 cm away from the source. At known time interval, the decomposed dye sample was withdrawn, centrifuged and then filtered. The quantitative analysis of CV was carried out using UV-Vis spectrophotometer (Hitachi U 2900, Tokyo, Japan) by measuring absorbance at 590 nm [35]. The photodegradation efficiency of CV dye was calculated according to the following equation,

$$\text{Efficiency} = C_0 - C / C_0 * 100 = A_0 - A_t / A_0 * 100. \quad (1)$$

**Table 1.** Variables and three levels.

	Low level (-1)	Medium level (0)	High level (+1)
<i>Independent variable</i>			
A = Conc. of dye (ppm)	5	7.5	10
B = Conc. of catalyst ( $\text{g l}^{-1}$ )	0.1	0.5	1.0
C = Reaction time (min)	0	60	120
<i>Dependent variable</i>			
Y1 = Photodegradation Efficiency or % degradation			

Various factors were evaluated in the degradation of CV dye using  $3^3$  level full-factorial design. The selection of 3 level factorial design is suitable for investigating the quadratic response surface model based on the second-order polynomial equation [36,37]. The independent variables selected were the concentration of dye (*A*, ppm), concentration of catalyst (*B*,  $\text{g l}^{-1}$ ) and reaction time (*C*, min), which were varied at three levels (-1, 0, +1). Table 1 shows  $3^3$  experimental design with 3 independent variables (*A*, *B*, *C*) at 3 different levels (-1, 0, +1) was used to study the effects on the dependent variable (*Y1*). The photodegradation efficiency (% , *Y1*) was selected as a dependent factor. The statistical experimental data were analysed using the Design-Expert® Software (Vers.-8.0.7.1, Stat-Ease Inc., Minneapolis).

## 2.6 Preparation of thick films

In this study, a thick film of PPy/1-D ZnO nanocomposite was used as a gas sensing module. The thixotropic pastes [38–41] were formulated by mixing the resulting fine powders with a solution of ethyl cellulose (a temporary binder) in a mixture of organic solvents such as butyl cellulose, butyl carbitol acetate and turpineol. The ratio of inorganic to organic part was kept at 75 : 25 in formulating the pastes. The thixotropic pastes were screen printed onto glass substrates in desired patterns. The films prepared were fired at  $90^\circ\text{C}$  for 2 h. Thus thick films of PPy/1-D ZnO nanocomposite were prepared. Silver contacts were made by vacuum evaporation for electrical and gas sensing measurements.

## 2.7 Gas sensor system

Gas sensing was performed by static gas sensing system, which comprises of 15 L glass gas chamber containing an electric heating plate, a thermocouple and a temperature controller. Required temperature conditions for sensing were maintained by heater resting on the base plate. The temperature was tuned by means of varying current through heater with adjustable ON and OFF time interval. Electrical connections and gas inlet were provided through ports at the base plate. The necessary gas concentration in the glass dome was achieved by injecting a required quantity of gas by means of a syringe. The current change was recorded by using a digital pico-ammeter keeping constant voltage. The sensing measurements were performed by exposing the thick films

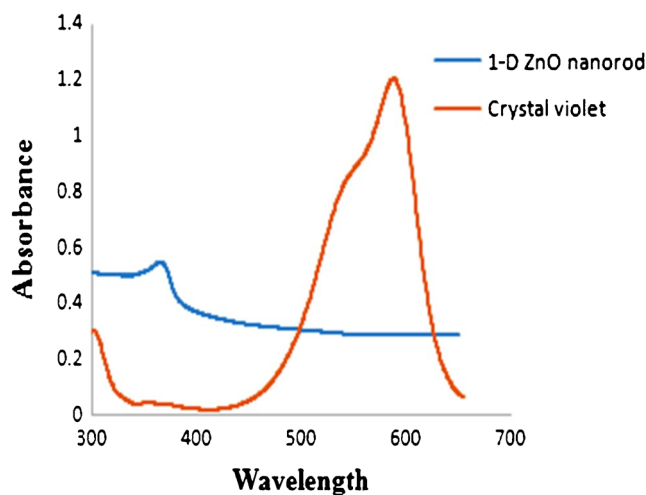


**Figure 1.** UV-Vis absorption spectra of 1-D ZnO nanorods and crystal violet.

of nanocomposite to gases in a closed glass dome (15 L) to mimic atmospheric condition. The electrical conductivity of a thick film in air and in the presence of gas was used to evaluate the sensor response as [38],

$$\text{Gas response } (s) = (G_a - G_g) / G_g, \quad (2)$$

where  $G_a$  is the conductance in the air and  $G_g$  the conductance upon exposure to test gas. Response time (RST) was defined as the time necessary to attain the 90% of the maximum increase in conductance subsequent to exposure of the sensing film to a gas, whereas recovery time (RCT) as the time needed to regain 90% of the maximum conductance in the air.

## 3. Results and discussion

### 3.1 UV-Vis absorption

The UV-Vis absorption spectra of synthesized 1-D ZnO nanorods and crystal violet are illustrated in figure 1. The precursor of ZnO synthesis shows the absorption spectra at 285.65 nm of zinc sulphate heptahydrate in the reported literature [42], after complete precipitation reaction with NaOH, it shows the absorption maxima at 361.5 nm of synthesized 1-D ZnO nanorods shown in figure 1. Similarly, crystal violet

showed the absorption maxima at 584.1 nm. The photocatalytic property involves the electron transition from the valence band to the conduction band resultant to the direct band gap of 1-D ZnO nanorods. The band gap energy of the 1-D ZnO nanorods was determined by the following equation [43],

$$E_g = hc/\lambda, \quad (3)$$

where  $h = 4.135 \times 10^{-15}$  eVs,  $c = 2.99 \times 10^8$  m s<sup>-1</sup> and  $\lambda = 361.5$  nm for 1-D ZnO nanorod synthesized by precipitation method. Applying above equation, the band gap energy of the synthesized 1-D ZnO nanorods was found to be 3.42 eV.

### 3.2 Field emission-scanning electron microscopy analysis

Field emission-scanning electron microscopy (FE-SEM) was performed to examine the surface characteristics of 1-D ZnO nanorods and PPy/1-D ZnO nanocomposite. Figure 2a shows uniform surface morphology of the 1-D ZnO nanorod with an average diameter of 30–50 nm. The synthesized 1-D ZnO nanorods were found to be isolated and free flowing in nature. The morphology of 1-D ZnO nanorods was changed after polymerization of pyrrole as shown in figure 2b. It was clear from the image that the 1-D ZnO nanorods were uniformly coated by polypyrrole. This revealed that the 1-D ZnO nanorods interact with PPy. The large area and uniform morphology of PPy/1-D ZnO nanocomposite are appropriate for gas sensing application [44].

### 3.3 Fourier transform infrared spectroscopy analysis

The Fourier transform infrared spectroscopy (FT-IR) spectra of 1-D ZnO nanorod and PPy/1-D ZnO nanocomposite

material are shown in figure 3. The IR spectrum of ZnO nanorods (figure 3a) showed the principle peaks at 3364.63 and 1553.71 cm<sup>-1</sup> and are due to the bending and stretching vibration of a hydroxyl group (–OH). The peak situated at 485.11 cm<sup>-1</sup> corresponds to the stretching vibration of Zn–O bond. The peaks at 1478 and 1558 cm<sup>-1</sup> are assigned to stretching mode of C=C and C–C in pyrrole ring are disappeared [45] and wide peak appears at 1536.35 cm<sup>-1</sup> in the PPy/1-D ZnO nanocomposite (figure 3b). The broadening and change in peak position indicate that there is a strong chemical interaction between PPy and 1-D ZnO nanorod.

### 3.4 X-ray diffraction

The XRD spectra of 1-D ZnO nanorod and PPy/1-D ZnO nanocomposite are shown in figure 4. From figure 4a, the XRD pattern of ZnO nanorods shows the characteristic peaks at scattering angles ( $2\theta$ ) of 30.78, 34.29, 35.34, 46.72, 54.74, 62.09 and 66.20° are correspond to the diffractions from (100), (002), (101), (102), (110), (103) and (112) crystal planes, respectively [21]. The sharp diffraction peaks implies the crystalline nature and no other peaks of impurity are observed in pure ZnO hexagonal (wurtzite) structure. The average crystallite size of 1-D ZnO nanorods is calculated by using Scherrer equation was found to be 20.13 nm. The XRD pattern of PPy/1-D ZnO nanocomposite is shown in figure 4b. This pattern exhibits a broad peak at a lower diffraction angle  $2\theta = 23.9$ , which implies their amorphous nature. This broadening of peak can be ascribed to the scattering of the PPy around 1-D ZnO nanorods [45].

### 3.5 Mechanism of photodegradation of crystal violet

In general, the UV light absorbed capacity of 1-D ZnO nanorods is more than any other nanostructures. This causes

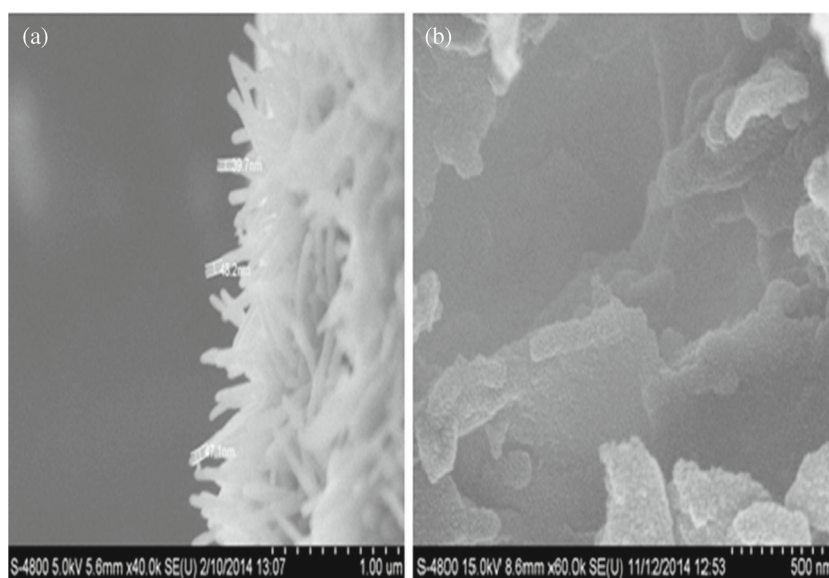


**Figure 2.** FESEM images of (a) 1-D ZnO nanorods and (b) PPy/1-D ZnO nanocomposites.



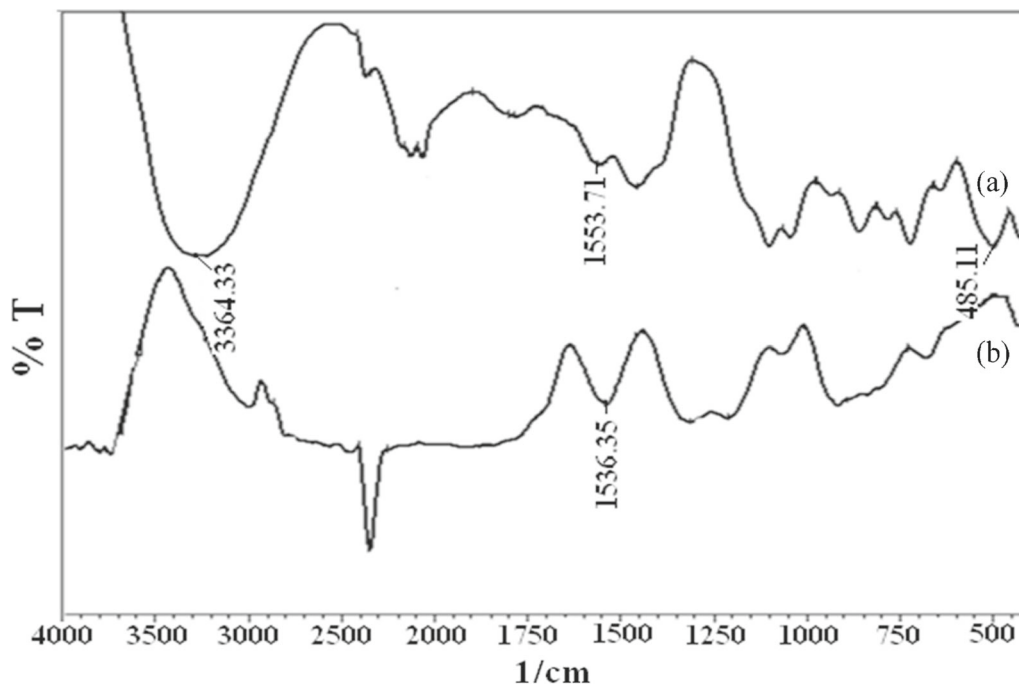


**Figure 3.** FTIR spectra of (a) 1-D ZnO nanorods and (b) PPy/1-D ZnO nanocomposites.

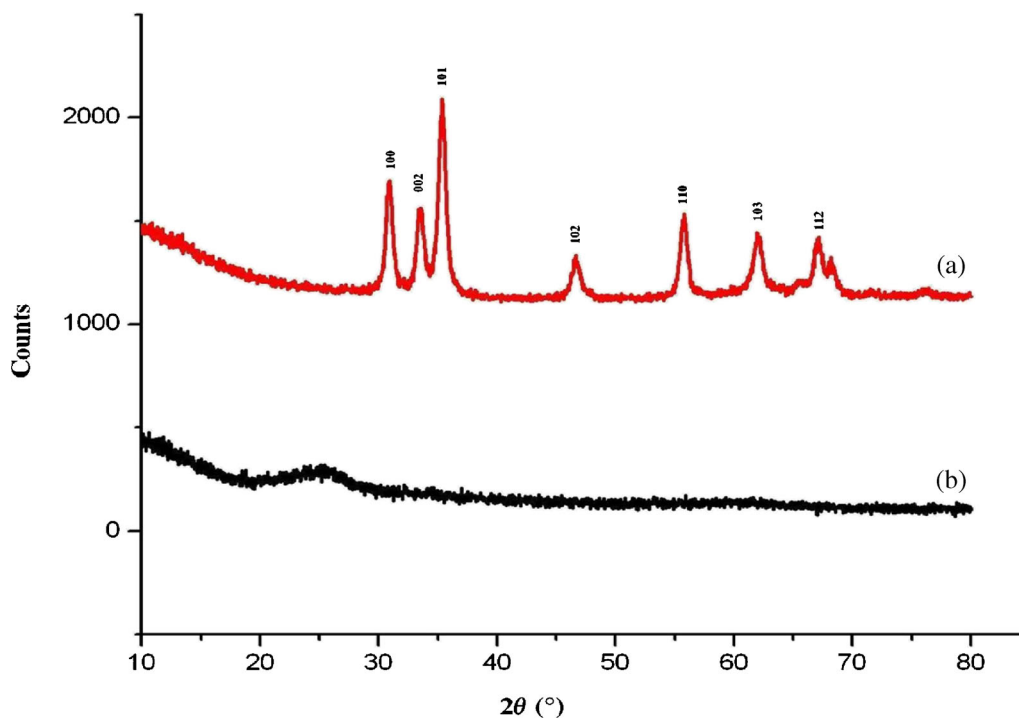
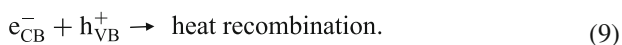
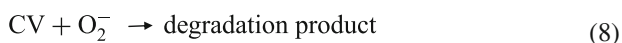
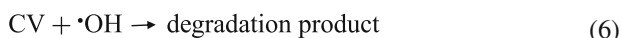
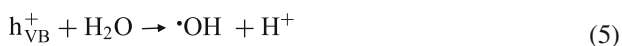


**Figure 4.** XRD pattern of (a) 1-D ZnO nanorods and (b) PPy/1-D ZnO nanocomposites.

the production of more electrons–hole ( $e^-/h^+$ ) pairs of conduction and valence band. This electron–hole pair plays an important role in the redox reaction. The highly oxidizing valence band holes react with  $H_2O$  to produce the

hydroxyl radicals and strongly reducing conduction band electrons produce the  $O_2^-$  molecules [46,47]. The hydroxyl radicals formed on the ZnO surface are strong oxidizing agents, which lead to the photodegradation of crystal violet.

The photodegradation reaction steps of crystal violet at the 1-D ZnO nanorod surface is described as follows [32],



### 3.6 Statistical analysis of photodegradation efficiency (%)

$3^3$  full-factorial experimental designs were used to evaluate the effect of independent variables on the dependent variables. Concentration of dye (*A*), concentration of catalyst (*B*) and reaction time (*C*) were selected as independent variables, while photodegradation efficiency (%), *Y1* was selected as a dependent variable. The effect of independent variables on dependent variable was investigated by deriving polynomial equation and contour plots. The photodegradation efficiency from different experimental runs is reported in table 2. Diagnostics case statistics for various response variables are shown in table 3. The polynomial equation obtained for (*Y1*),

$$Y1 = 64.41 - 17.28A - 0.16B + 1.26C + 0.99A^2 - 8.63B^2 - 3.97C^2 + 2.18AB - 0.016AC + 0.13BC.$$

A positive value in the above equation represents the synergistic effect of the independent variable, while a negative

**Table 2.** Photodegradation efficiency (%), *Y1*.

Batch no.	Conc. of dye (ppm)	Conc. of catalyst (g l <sup>-1</sup> )	Reaction time (min)	Photodegradation efficiency (%)
F1	7.50	0.10	120.00	74.59
F2	7.50	1.00	60.00	59.91
F3	7.50	0.50	60.00	52.74
F4	7.50	0.50	60.00	53.50
F5	7.50	0.50	60.00	54.00
F6	10.00	0.10	60.00	34.80
F7	7.50	0.10	0.00	0.00
F8	10.00	1.00	0.00	0.00
F9	5.00	0.50	60.00	75.44
F10	7.50	0.50	60.00	54.50
F11	10.00	1.00	60.00	67.90
F12	7.50	0.50	60.00	52.74
F13	7.50	1.00	120.00	92.95
F14	10.00	0.10	120.00	72.60
F15	10.00	0.10	0.00	0.00
F16	7.50	1.00	0.00	0.00
F17	5.00	0.50	0.00	0.00
F18	5.00	0.10	60.00	63.87
F19	5.00	1.00	120.00	97.13
F20	5.00	0.50	120.00	92.53
F21	10.00	0.50	60.00	53.62
F22	5.00	0.10	120.00	93.68
F23	5.00	1.00	60.00	84.40
F24	7.50	0.50	60.00	54.75
F25	7.50	0.10	60.00	38.78
F26	10.00	0.50	120.00	88.00
F27	7.50	0.50	0.00	0.00
F28	5.00	0.10	0.00	0.00
F29	7.50	0.50	120.00	89.19
F30	10.00	0.50	0.00	0.00
F31	10.00	1.00	120.00	93.71
F32	5.00	1.00	0.00	0.00

**Table 3.** Diagnostic case statistics of response variable (*Y1*).

Batch no.	Actual value	Predicted value	Residual
F1	74.59	73.86	0.73
F2	59.91	60.51	-0.60
F3	52.74	54.97	-2.23
F4	53.50	54.97	-1.47
F5	54.00	54.97	-0.97
F6	34.80	45.94	-11.14
F7	0.00	-7.64	7.64
F8	0.00	4.24	-4.24
F9	75.44	66.74	8.70
F10	54.50	54.97	-0.47
F11	67.90	63.93	3.97
F12	52.74	54.97	-2.23
F13	92.95	93.96	-1.01
F14	72.60	69.94	2.66
F15	0.00	-6.71	6.71
F16	0.00	-1.59	1.59
F17	0.00	6.12	-6.12
F18	63.87	61.38	2.49
F19	97.13	105.42	-8.29
F20	92.53	98.70	-6.17
F21	53.62	55.66	-2.04
F22	93.68	90.22	3.46
F23	84.40	69.55	14.85
F24	54.75	54.97	-0.22
F25	38.78	47.43	-8.65
F26	88.00	82.79	5.21
F27	0.00	-3.22	3.22
F28	0.00	3.89	-3.89
F29	89.19	84.52	4.67
F30	0.00	-0.12	0.12
F31	93.71	94.96	-1.25
F32	0.00	5.02	-5.02

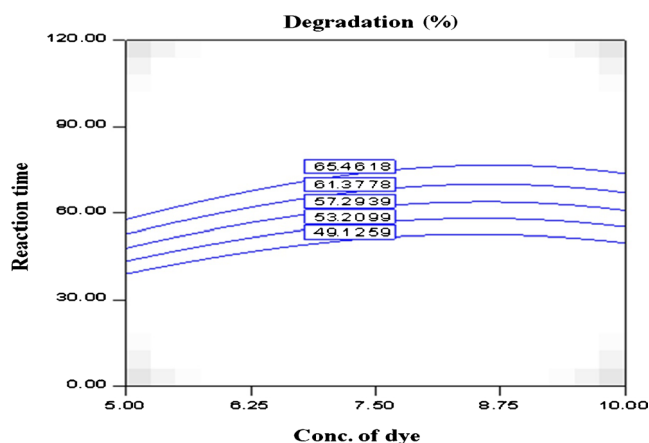
**Table 4.** Summary of regression analysis for response Y1.

Models	$R^2$	Adjusted $R^2$	Predicted $R^2$	Std. Dev.	Press	Remarks
Response Y1						
Linear	0.9265	0.9187	0.9000	10.14	3917.17	.....
2FI	0.9340	0.9181	0.8793	10.17	4731.25	.....
Quadratic	0.9764	0.9667	0.9411	6.49	2309.91	Suggested
Cubic	0.9943	0.9882	0.9643	3.86	1398.85	.....

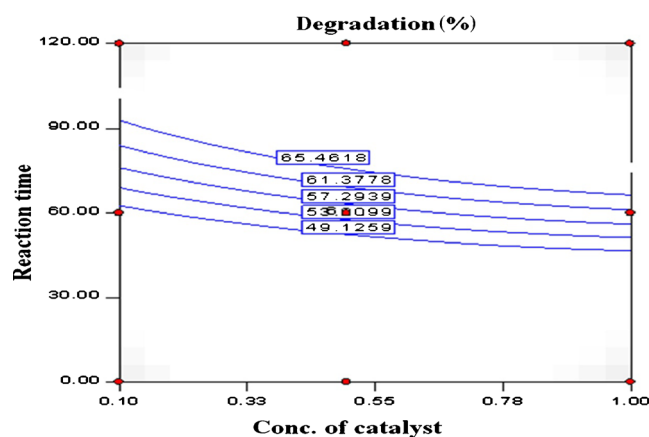
$$Y1 = 64.41 - 17.28A - 0.16B + 1.26C + 0.99A^2 - 8.63B^2 - 3.97C^2 + 2.18AB - 0.016AC + 0.13BC.$$

**Table 5.** ANOVA of model for Y1.

Source	DF	Sum of squares	Mean square	F-value	P-value
Model for Y1	9	38260.17	4251.13	101.07	<0.0001
A	1	498.08	498.08	11.84	<0.0023
B	1	769.37	769.37	18.29	0.0003
C	1	35192.87	35192.87	836.71	<0.0001
A <sup>2</sup>	1	277.39	277.39	6.59	0.0175
B <sup>2</sup>	1	21.21	21.21	0.50	0.4851
C <sup>2</sup>	1	1467.61	1467.61	34.89	<0.0001
AB	1	72.65	72.65	1.73	0.2023
AC	1	70.23	70.23	1.67	0.2097
BC	1	149.01	149.01	3.54	0.0731


**Figure 5.** Effect of individual variables (conc. of dye and reaction time) on degradation efficiency (%).

value represents the inverse relationship (antagonistic effect) [48,49].  $-17.28$  represents the antagonistic effect of independent factor A (concentration of dye) on photodegradation efficiency (%). While  $+1.26$  represents the synergistic effect of independent factor C (reaction time) on photodegradation efficiency (%). The suggested model for the Y1 was found to be quadratic as per design expert software with  $R^2 = 0.9764$ , which is shown in table 4. The P-value for the Y1 model was found to be  $<0.0001$ , which clearly indicates the model is statistically significant


**Figure 6.** Effect of individual variables (conc. of catalyst and reaction time) on degradation efficiency (%).

( $P < 0.05$  indicates that model terms are significant). The results showed that the photodegradation efficiency of CV dye was affected by the independent variables. Table 5 shows the ANOVA of model for Y1. The effect of A ( $P < 0.0023$ ), B ( $P = 0.0003$ ), C ( $P = 0.0001$ ) and C<sup>2</sup> ( $P = 0.0001$ ) were found to be statistically significant. The interaction terms AB in Y1 show how photodegradation efficiency changes when 2 variables are simultaneously changed. The model F-value for Y1 was 101.07, which implies that the model was significant. To analyse the effect of independent variables on the dependent variable, a 2D contour plot was constructed for the photodegradation efficiency of CV dye. From the contour plot (figure 5), it was observed that the photodegradation efficiency of CV dye was increased from lower level to a higher level of dye concentration (A) and reaction time (C). The same type of results was observed in the case of catalyst concentration (B) and reaction time (C) from contour plot (figure 6). From contour plot (figure 7), it could be concluded that when the concentration of the catalyst (B) was kept constant and the concentration of dye (A) was increased, the photodegradation efficiency of CV dye decreases. This might be due to an increase in concentration of dye which decreases the path length of photons that arrive in the solution, therefore only few photons reached the catalyst surface, which decreases the production rate of hydroxyl and superoxide radical formation [50]. Also, when the concentration of

dye (A) was kept constant and concentration of catalyst was increased, the photodegradation efficiency of crystal violet increases. This may be due to an increase in concentration of catalyst, increases the active sites available on photocatalyst surface for the reaction, which successively increases the production rate of hydroxyl and superoxide radical formations [32,50]. The degradation performance of the nanomaterials was studied by various scientists and its performance in terms of % degradation and time interval was compared with the present study, shown in table 6.

### 3.7 Gas sensing mechanism

The mechanism for gas detection in nanomaterials is based on reactions that occur at the active sites of the sensor surface, resulting in a change in the concentration of adsorbed oxygen ( $O^-$ ) ions. Oxygen ions adsorb onto the material's surface, capture electrons from the bulk, building a potential barrier of depth  $\delta$  that decreases the channel width  $L_c$  of passage of electrons through a nanoparticle of diameter  $D$  and hence, decrease in electron movement and the conductivity occurs [51].

$$L_c = D - 2\delta. \quad (10)$$

If the particle size is reduced up to nanometer level (<100 nm), the channel width would be almost blocked and the initial resistance of the sensor would be infinitely high

in air ambient. On exposure, the target gas would consume oxygen atoms to oxidize, liberating electrons behind it on the surface. Desorption of oxygen from the surface of the sensor would decrease the potential barrier height, which broadens the channel width for migration of electrons. Thus, nanoscaled materials offer the grain sizes where the depletion layer has about the same dimensions as the particle radii. The charge transfer is, therefore, predominantly grain-controlled. When reactive gases combine with this oxygen, the barrier height is reduced, broadening the passage of electrons and hence, conductivity increases. This change in conductivity is directly related to the amount of a specific gas present in the environment, resulting in a quantitative determination of gas presence and concentration. To maximize the opportunities for surface reactions, a high ratio of surface area to volume is needed. As an inverse relationship exists between surface area and particle size, nanoscale materials, which exhibit very high surface area, are highly desirable.

### 3.8 Gas sensing measurements

3.8a *Selectivity*: Figure 8 shows gas selectivity performance of PPy/1-D ZnO nanocomposites at room temperature. It can be seen that PPy/ZnO-15 is highly selective towards  $NH_3$  gas. In addition, the decrease in selectivity to ammonia was observed to increase the mass% of 1-D ZnO nanocomposite.

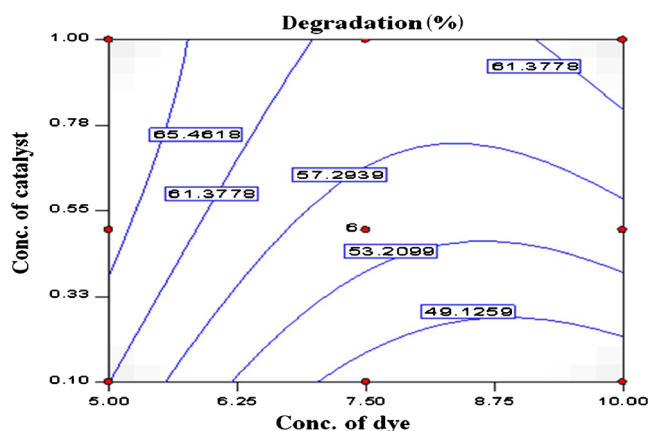


**Figure 7.** Effect of individual variables (conc. of dye and conc. of catalyst) on degradation efficiency (%).

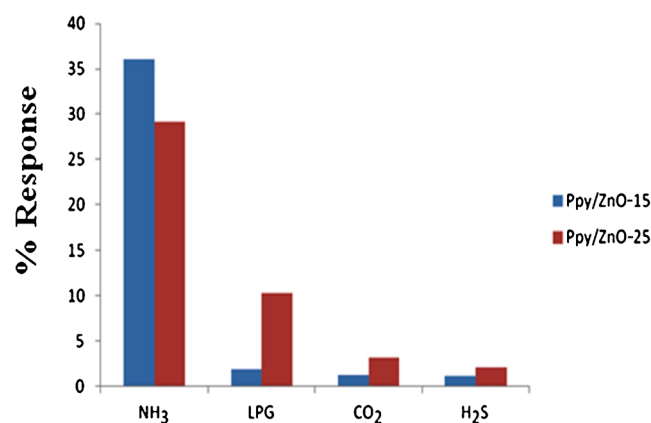


**Figure 8.** Selectivity performance of PPy/1-D ZnO nanocomposite.

**Table 6.** Comparative degradation performance of the nanomaterials.

Catalyst	Degradation material	Source	Degradation (%)	Time interval (min)
ZnO [35]	Crystal violet	UV light	96	80
ZnO [52]	Reactive red 120	Solar light	100	60
1-D ZnO (present study)	Crystal violet	UV light	97.13	120
TiO <sub>2</sub> [53]	Crystal violet	UV light	100	30



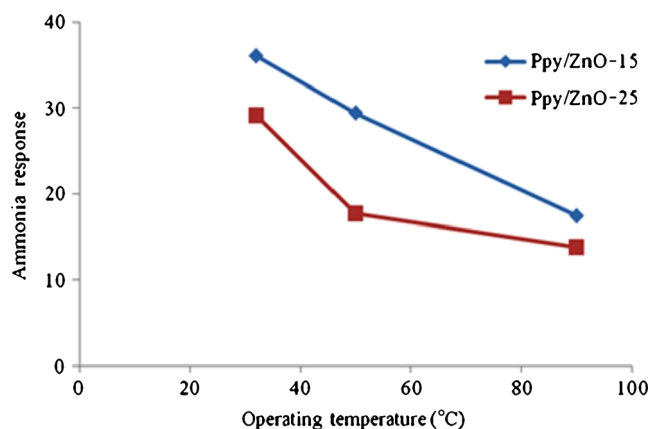


**Figure 9.** Variation of ammonia response with operating temperatures.

**3.8b Effect of operating temperature:** For the gas sensing study, we prepare two nanocomposite PPy/ZnO-15 and PPy/ZnO-25, where 15 and 25 are the mass percentages of 1-D ZnO nanorods in the nanocomposite. The response of PPy/1-D ZnO nanocomposite thick films to 1000 ppm of  $\text{NH}_3$ , as a function of operating temperature, is shown in figure 9. It is observed from the figure that the gas response is highest at room temperature and decreases with operating temperature. The sample, PPy/ZnO-15 showed the highest response to 1000 ppm  $\text{NH}_3$  at room temperature ( $32^\circ\text{C}$ ). The response to ammonia could be attributed to the surface active sites to sense ammonia gas.

**3.8c Effect of gas concentration (ppm):** The change in response of PPy/ZnO thick film with variation in gas concentration is shown in figure 10a and b. The highest

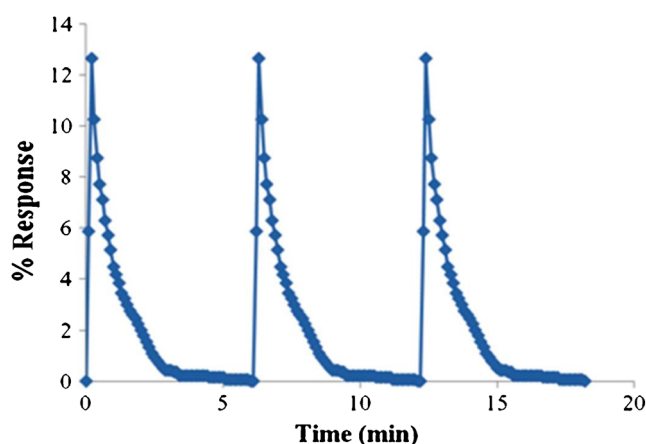


**Figure 11.** Response and recovery profile of PPy/ZnO-15 nanocomposite.

response recorded were 36.1 and 29.19% for 1000 ppm of  $\text{NH}_3$  at room temperature for PPy/ZnO-15 and PPy/ZnO-25, respectively. It was observed that the increase in ZnO doping results in a decrease in the response of sensing film. Response of sensing film to  $\text{NH}_3$  was found to be decreased with increase in temperature. However, interestingly, recovery time was found to be decreased at elevated temperature, although at  $90^\circ\text{C}$  only  $\sim 89\%$  of original conductance was recovered.

**3.8d Response–recovery profile of the sensor:** Recovery time of PPy/ZnO-15 sensing film was 2, 6 and 10 min for 300, 600 and 1000 ppm of  $\text{NH}_3$ , respectively, at  $50^\circ\text{C}$  after introduction of clean air. The reproducing capability of nanocomposite was investigated by exposing it to 300 ppm at  $50^\circ\text{C}$  and then blowing air repeatedly for three

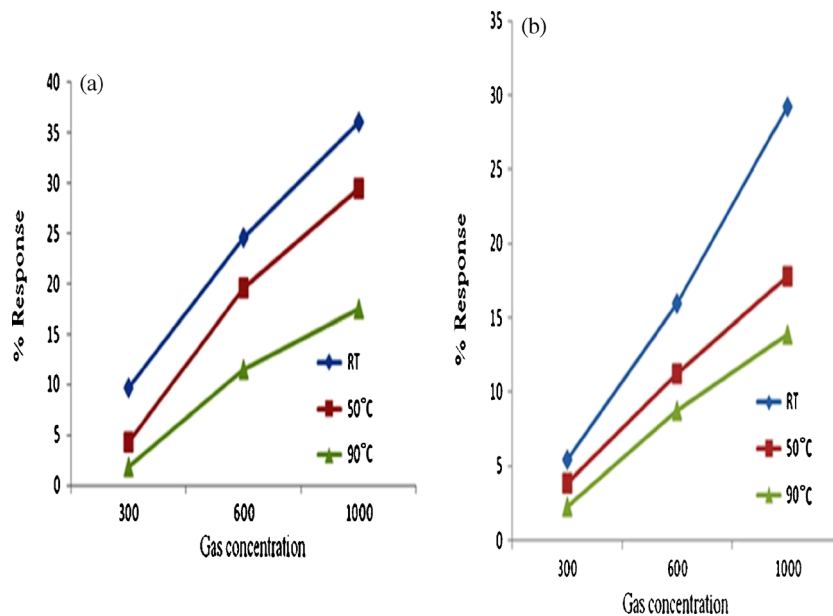


**Figure 10.** Response of (a) PPy/ZnO-15 and (b) PPy/ZnO-25 nanocomposites to ammonia at different gas concentrations.

**Table 7.** Comparative gas sensing performance of the nanocomposites/nanomaterials.

Nanomaterial/ nanocomposite	Gas	Sensitivity (%)	Response time	Recovery time
PPy/ZnO [54]	NO <sub>2</sub> (100 ppm)	38	2–4 min	24 h
PPy/ZnO [45]	LPG (1400 ppm)	32.5	3.5–4 min	40 min
ZnO nanorod [55]	NH <sub>3</sub> (50 ppm)	97.7	14 s	25 s
1-D ZnO nanorod/PPy (present study)	NH <sub>3</sub> (1000 ppm)	36.1	2–5 s	10 min
PPy [56]	NH <sub>3</sub> (25 ppm)	16	20 s	15 min

times. It was observed from figure 11 that the PPy/ZnO-15 nanocomposite showed excellent recovery. The gas sensing performance of the nanocomposites/nanomaterials was studied by various scientists and its performance in terms of sensitivity, response and recovery time was compared with present study as shown in table 7.

#### 4. Conclusion

1-D ZnO nanorods were successfully synthesized by surfactant-assisted precipitation method using ZnSO<sub>4</sub>·7H<sub>2</sub>O as precursor, which serve as photocatalyst for the degradation of crystal violet dye. 3<sup>3</sup> full-factorial experimental design was used to evaluate the effect of independent variables on the photodegradation efficiency (%). The photocatalytic activity of synthesized 1-D ZnO nanorods shows very rapid degradation of crystal violet dye with the degradation rate of 97.13% was achieved by run F19 using 5 ppm concentration of dye, 1 g l<sup>-1</sup> concentration of catalyst and reaction time interval of 120 min. This might be due to an increase in concentration of catalyst, increases the active sites available on photocatalyst surface for the reaction. However, the catalyst concentration less than 1 g l<sup>-1</sup> restricts the degradation rate of crystal violet at 5 ppm of dye concentration. The present result suggests that the 3<sup>3</sup> full-factorial experimental design was reliable for optimizing the degradation rate of crystal violet by the 1-D ZnO nanorods. On the other hand, PPy/1-D ZnO nanocomposite was successfully prepared by *in situ* polymerization of pyrrole monomer. The synthesized PPy/ZnO-15 nanocomposite showed high sensitivity and selectivity towards NH<sub>3</sub> (36.1%) at room temperature. During study, it was found that increase in concentration of 1-D ZnO in nanocomposite resulted in a decrease in sensitivity as well as recovery time. Owing to high sensitivity and good recovery time at room temperature, the proposed nanocomposite holds great promises in the gas sensor field.

#### Acknowledgement

We are grateful to Technical Education Quality Improvement Programme (TEQIP-II) for providing financial assistance to carry out this research work.

#### References

- [1] Tian F, Zhao Y, Liu Y, Cao H, Zhao J and Lu X 2014 *Mater. Lett.* **119** 8
- [2] Okada T, Kawashima K and Nakata Y 2006 *Thin Solid Films* **506** 274
- [3] Rao C, Kulkarni G, Thomas P and Edwards P 2000 *Chem. Soc. Rev.* **29** 275
- [4] Deng Z, Chen M, Gu G and Wu L 2008 *J. Phys. Chem. B* **112** 16
- [5] Yang S and Park C 2008 *Nanotechnology* **19** 4
- [6] Krishnakumar T, Jayaprakash R, Pinna N, Singh V, Mehta B and Phani A 2008 *Mater. Lett.* **63** 242
- [7] Li M, Bala H, Lv X, Ma X, Sun F and Tang L 2007 *Mater. Lett.* **61** 690
- [8] Patzake G, Krumeich F and Nesper R 2002 *Angew. Chem. Int. Ed.* **419** 2446
- [9] Cao B and Cai W 2008 *J. Phys. Chem. C* **112** 680
- [10] Kundu S 2014 *Colloids Surface A* **446** 199
- [11] Nithiyanantham U and Kundu S 2014 *Ind. Eng. Chem. Res.* **53** 13667
- [12] Shen W, Li Z, Wang H, Liu Y, Guo Q and Zhang Y 2008 *J. Hazard Mater.* **152** 172
- [13] Ba-Abbad M M, Kadhum A A H, Mohamad A B, Takriff M S and Sopian K 2013 *Chemosphere* **91** 1604
- [14] Baruah S, Jaisai M, Imani R, Nazhad M and Dutta J 2010 *Sci. Technol. Adv. Mater.* **11** 7
- [15] Hong R Y, Li J H, Chen L L, Liu D Q, Li H Z, Zheng Y and Ding J 2009 *Powder Technol.* **189** 426
- [16] Yadav B C, Srivastava R and Kumar A 2007 *Int. J. Nanotechnol. App.* **1** 1
- [17] Jothi N S, Gunaseelan P and Sagayaraj P 2012 *Arch. Appl. Sci. Res.* **4** 1698
- [18] Chen Z, Wang T, Jin X, Chen Z, Megharaj M and Naidu N 2013 *J. Colloid Interf. Sci.* **398** 59
- [19] Ovejero G, Rodríguez A, Vallet A, Willerich S and García J 2012 *Appl. Catal. B* **111** 586
- [20] Chen C C, Liao H J, Cheng C Y, Yen C Y and Chung Y C 2007 *Biotechnol. Lett.* **29** 391
- [21] Kanmoni V G, Daniel S and Raj G A 2012 *Reac. Kinet. Mech. Cat.* **106** 325
- [22] Baruwati B, Kumar D K and Manorama S V 2006 *Sens. Actuators B* **119** 676
- [23] Karin P K 2002 *Crit. Rev. Anal. Chem.* **32** 121

- [24] Saxena V, Aswal D, Kaur M, Koiry S, Gupta S, Yakhmi J *et al* 2007 *Appl. Phys. Lett.* **90** 1077
- [25] Patil D R and Patil L A 2006 *Sens. Transducers* **70** 661
- [26] Chabukswar V V, Pethkar S and Athawale A A 2001 *Sens. Actuators B* **77** 657
- [27] Lahdesmaki G, Lewenstam A and Ivaska A 1996 *Talanta* **43** 125
- [28] Wang X, Miura N and Yamazoe N 2000 *Sens. Actuators B* **66** 74
- [29] Xu C N, Miura N, Ishida Y, Matuda K and Yamazoe N 2000 *Sens. Actuators B* **65** 163
- [30] Wang Y, Wu X, Su Q, Lee Y and Zhou Z 2001 *Solid State Electron.* **45** 347
- [31] Moseley P T and Williams D E 1990 *Sens. Actuators B* **1** 113
- [32] Selvam N C S, Narayanan S, Kennedy L J and Vijaya J J 2013 *J. Environ. Sci.* **25** 2157
- [33] Kumar S S, Venkateswarlu P, Rao V R and Rao G N 2013 *Int. Nano Lett.* **3** 1
- [34] Batool A, Kanwal F, Imran M, Jamil T and Siddiqi S A 2012 *Synth. Met.* **161** 2753
- [35] Ameen S, Akhtar M S, Nazim M and ShikShin H 2013 *Mater. Lett.* **96** 228
- [36] Roy P and Shahiwala A 2009 *Eur. J. Pharm. Sci.* **37** 363
- [37] Vaghasiya H, Kumar A and Sawant K 2013 *Eur. J. Pharm. Sci.* **49** 311
- [38] Patil D R, Patil L A and Patil P P 2007 *Sens. Actuators B* **126** 368
- [39] Hankare P P, Sanadi K R, Garadkar K M, Patil D R and Mulla I R 2013 *J. Alloys Compd.* **553** 383
- [40] Gawas U B, Verenkar V M S and Patil D R 2011 *Sens. Transducers* **134** 45
- [41] Patil R P, Nikam P N, Delekar S D, Patil D R and Hankare P P 2014 *Sens. Lett.* **12** 01
- [42] Kanagadurai R, Durairajan R, Sankar R, Sivanesan G, Elangovan S P and Jayavel R 2009 *E.-J. Chem.* **6** 871
- [43] Sharma D, Sharma S, Kaith B, Rajput S and Kaur M 2011 *Appl. Surf. Sci.* **257** 9661
- [44] Chougule M A, Sen S and Patil V B 2012 *Synth. Met.* **162** 1598
- [45] Barkade S S, Pinjari D V, Singh A K, Gogate P R, Naik J B, Sonawane S H *et al* 2013 *Ind. Eng. Chem. Res.* **52** 7704
- [46] Chena C C, Fan H J, Jang C Y, Jan J L, Lin H D and Lua C H 2006 *J. Photoch. Photobiol.: A* **184** 147
- [47] Khezrianjoo S and Revanasiddappa H D 2013 *J. Catal.* Article ID 582058
- [48] Gannu R, Yamsani V V, Yamsani S K, Palem C R, Yamsani M R 2009 *AAPS Pharm. Sci. Tech.* **10** 505
- [49] Nayak A K, Pal D, Pradhan J and Hasnain M S 2013 *Int. J. Biol. Macromol.* **54** 144
- [50] Byrappa K, Subramani A K, Ananda S, Rai K M L, Dinesh R and Yoshimura M 2006 *Bull. Mater. Sci.* **29** 433
- [51] Patil D R 2007 Studies on ZnO based gas sensors Ph.D Thesis
- [52] Velmurugan R and Swaminathan M 2011 *Sol. Energ. Mat. Sol. C* **95** 942
- [53] Senthilkumaar S and Porkodi K 2005 *J. Colloid. Interf. Sci.* **288** 184
- [54] Chougule M A, Dalvi D S, Mali S, Patil P S, Moholkar A V, Agawane G L *et al* 2012 *Measurement* **45** 1989
- [55] Dighavkar C 2013 *Arch. Appl. Sci. Res.* **5** 96
- [56] Joshi A, Gangal S A and Gupta S K 2011 *Sens. Actuators B* **156** 938